Journal of Superconductivity and Novel Magnetism (2023) 36:131–146
https://doi.org/10.1007/s10948-022-06431-1

ORIGINAL PAPER

The Structural, Electronic, Magnetic, Mechanical, and Lattice Dynamical Properties of the Novel Full-Heusler Alloys Mn_2HfX (X = Si and Ge): Ab Initio Study

Mohamed Lamine Belkhir[1] · Ahmed Gueddouh[1,2] · Fares Faid[1,2] · Mourad Rougab[1,2]

Received: 10 September 2022 / Accepted: 10 October 2022 / Published online: 5 November 2022

Abstract
Through first-principles investigation, two new Mn_2-based full-Heusler alloys, Mn_2HfSi and Mn_2HfGe, have been studied using the full-potential linearized augmented plane wave (FP-LAPW) approach as implemented in the WIEN2k code. Our study focuses on these compound's stability (thermodynamic, dynamic, and mechanical), electronic, and magnetic properties. The $L2_1$ (Cu_2MnAl-type) structure is shown to be more energetically favorable than the XA (Hg_2CuTi-type) structure for both compounds, Mn_2HfX (X = Si and Ge). We demonstrate that Mn_2HfX (X = Si and Ge) are stable through the calculations of cohesive, formation energies, phonon dispersion curves, and the elastic constants, with the illustration of 3D and 2D bulk and Young's moduli. Using GGA and GGA-mBJ calculations show that Mn_2HfX (X = Si and Ge) are half-metallic ferrimagnets (HMFs), with indirect band gap through the altered Becke-Johnson (mBJ), GGA approximation: 0.689 eV for Mn_2HfSi and 0.520 eV for Mn_2HfGe. Furthermore, the electrons at the Fermi level (E_F) were fully spin-polarized. The total magnetic moment in these two compounds was found to have an integer value of 2 μ_B per formula, which complies with the Slater-Pauling rule $M_{tot} = Z_{tot} - 24$. These compounds are favorable materials for spintronic applications. It was revealed that Mn_2HfSi and Mn_2HfGe maintained their half-metallicity for lattice constants in the range of 5.7–6.2 Å and 5.75–6.2 Å, respectively.

Keywords DFT · Wien2K · Full-Heusler alloys · Half metallic · Slater-Pauling · Ferrimagnetic · Spintronic

1 Introduction

Heusler alloys (HAs) have a more comprehensive range of applications, such as spintronic application, optoelectronic, topological insulator, and thermoelectric applications [1–3]. Among the essential characteristics of HAs, which have attracted much care in the last years, is the behavior of half-metallic [4]. At Fermi level (E_F), we find that one spin direction displays a gap, while the other displays metallic behavior, leading to full spin polarization. Alloys with half-metallic behavior are much required in the spintronic field, which is one of the most reliable and promising emerging technologies in magnetic (multilayer) films [5]. The half-metallic property is not exclusive to Heusler alloys but relatively recently appeared distinctively in two-dimensional compounds [6–8]. As an example of the application of this field; tunnel magnetoresistance (TMR) and giant magnetoresistance (GMR) [2, 9, 10]. Following the Slater-Pauling (SP) rule [11], it is also possible to predict a feature of a perfect half-metal in HAs by possessing an integer magnetic moment. In the $L2_1$ full-Heusler compounds, as in our case, the SP relation becomes $M_{tot} = Z_{tot} - 24$ [12], where M_{tot} is the total spin magnetic in the unit cell scales and Z_{tot} is the total number of valence electrons per unit cell, while for the half-Heusler compounds, this relation becomes $M_{tot} = Z_{tot} - 18$ [13].

The HAs with the form X_2YZ, crystallizing in the $L2_1$ structure with prototype Cu_2MnAl, and the inverse Heusler XA structure with prototype Hg_2CuTi are members of the Heusler alloy family. Half-Heusler alloys (ternary and quaternary) have the XYZ ($XX'YZ$) formula. When one of the two X atoms is replaced by a different transition metal, X',

✉ Ahmed Gueddouh
a.gueddouh@lagh-univ.dz

[1] Laboratoire de Physique Des Matériaux, Université Amar Telidji de Laghouat, BP37G03000 Laghouat, Algeria

[2] Department of Science and Technology – Common Core, University Amar Telidji of Laghouat, Laghouat, Algeria

a quaternary compound with the formula *XX'YZ* is formed. Here, *X* represents a high-valent transition or noble metal atom, *Y* is a low-valent transition metal atom, and *Z* is an sp element.

Regarding the Mn_2-based complete Heusler, the Mn atom's position in the periodic table provided her the option to crystallize in either the regular or inverse Heusler. These configurational selections are made based on the valence electrons and electronegativity of the *X* and *Y* atoms. For more precise information about the Mn_2YZ, we discuss all possibilities. Firstly, we started with literature and the known variety of spin alignments [14, 15]. The compounds with *X* = Mn and *Y* atoms with a valence lower than Mn have Ferro magnetically (FM—all parallel spins) coupled Mn atoms or are nonmagnetic (NM) (Mn_2MoGe, Mn_2MoSn, Mn_2WGa, Mn_2WIn, and Mn_2WSb) in the regular stable phase [12]. The current trend that we highlighted in our study is that Mn_2YZ have ferrimagnetically (FIM-several spins up and some down) coupled Mn atoms with a low magnetic moment. Among the HAs in the half-metallic ferrimagnets (HMFIs) order, full Heusler based on Mn_2 that contains *Y* from a 3d, 4d, or 5d transition element and *Z* being an sp element is of particular importance. In contrast to the literature, which declares that the majority of Mn_2-based full Heusler are ferromagnetic (FM) in regular phases and the ferrimagnetic found in inverse phases, previous studies have discovered some compounds in the regular phase with ferrimagnetic states, such as Mn_2ZrSi and Mn_2ZrGe [16]. The anti-parallel alignment of two Mn magnetic moments in a ferrimagnetic structure HMFIs is a fascinating family of HAs that have gotten a lot of greater significance because this is due mainly to the system's low total magnetic moment, which provides extra benefits [17]. They do not generate a lot of stray fields in electronics, are less affected by external magnetic fields, and have demonstrated that particular materials can exhibit ferrimagnetism. Mn_2YZ Heusler alloys are a potential material in future spintronic devices like efficient spin-transfer torque [18], because of strong electron-spin polarization with high Tc [19].

Ruben Weht and Warren E. Pickett theoretically and experimentally explored one of the HMFIs, Mn_2Val [19, 20], and then K. Ozdogan and I. Galanakis demonstrated the HMFIs behavior of Mn_2VZ (*Z* = Al, Ga, In, Si, Ge, Sn) with several sp elements [21]. In this regard, Hongzhi et al. predicted half-metallic characteristics for the HAs Mn_2CrZ (*Z* = Al, Ga, Si, Ge, Sb) [22] and added more compounds to the list of HMFIs. Subsequently, Li et al. and Wei et al. [23, 24] examined the electronic structure and magnetism of Mn_2CuAl and Mn_2CuGe. Further, lately, Meinert et al. [17] researched several Mn_2TiZ compounds using simulation studies that illustrated the behavior of HMFIs. While Liu et al. investigated the Mn_2NbSi full-Heusler combination [25], new HMFIs Mn_2ZrSi and Mn_2ZrGe were investigated by Abada et al. [16]. In addition, Benaddi et al. studied the rise of the HMFIs full-Heusler combination in Mn_2IrGe [26]; in addition, new Heusler alloys Mn_2ScZ (*Z* = Si, Ge, Sn) were investigated by Ram et al. [27]. Also, Ram et al. studied structural and mechanical properties in the inverse Heusler alloy $Mn_2ZnSi_{(1-x)}$ Ge_x [28]. Sokolovskiy et al. have demonstrated the ferrimagnetic nature of Mn_2NiZ (*Z* = Ga, In, Sn, Sb) alloys [29]. Predictions of the half-metallic, mechanical, and acoustic properties of Hg_2CuTi-type in Mn_2LiZ (*Z* = As, Sb) compounds were investigated by Jiang et al. [30] as well as the electronic structure, magnetism, and thermoelectricity of new Mn_2(Y, Zn)Sn Heusler compounds by Yousuf and Gupta [31]. Huijun et al. studied the structural, elastic, electrical, and magnetic characteristics of the new full-Heusler Mn_2MgGe alloy [32], while Maizia et al. researched the new full-Heusler Mn_2OsGe HMFIs alloy [33].

Until recently, the bulk of Mn_2YZ Heusler alloys that have been studied had 4d transition metal components in the *Y* position. Much study has not been done on Mn_2-based Heusler compounds containing 5d transition metal components. This study's main objective is to utilize first-principles calculations to compute the electronic structures and magnetic characteristics of Mn_2HfSi and Mn_2HfGe Heusler compounds with $AlCu_2Mn$-type structures and employ them to forecast new HMFIs compounds. There are no comparable experimental studies or theoretical data to our knowledge.

2 Calculation Method

The structural, electronic, and magnetic properties of full-Heusler Mn_2HfX (*X* = Si, Ge) have been investigated using first-principles FP-LAPW (full-potential linearized augmented plane wave) [33] as employed in the WIEN2k code [34]. We have adopted the generalized gradient approximation in the Perdew-Burke-Ernzerhof form (GGA-PBE) [35, 36]. The threshold energy between core states and valence states was −7.0 Ry. The $R_{mt}K_{max}$ is chosen equal to 9, which determines the matrix size (convergence), where K_{max} is the plane wave cut-off, R_{mt} is the smallest of all atomic sphere radii, and the $G_{max} = 14$ (a.u-1). The choice of muffin-tin radii (RMT) is made so that the interstitial region between the different spheres is the smallest to ensure the accuracy of our calculations. Selected RMT values are 2.30 for Mn and 2.38 for Hf, and for Si and Ge, 2.16 and 2.25. The irreducible Brillouin zone (IBZ) k-point number has been set at 4000. The Mn:(Ar) $3d^5 4s^2$, Hf:(Xe) $5d^2 6s^2$, Si:(Ne) $3s^2 3p^2$, and finally, Ge:(Ne)$3s^2 3p^2$ electrons are presented as valence electrons. Also, Tran and Blaha-modified Becke-Johnson (TB-mBJ) potential was used to predict the band gap results with more accuracy [37]. The convergence criteria for the total energy have been taken as 10^{-4} eV. Phonon spectra are calculated by the pseudo-potential-based Quantum Espresso package [38] within the framework of GGA-PBE.

3 Results and Discussion

3.1 Structural and Thermodynamic Properties

3.1.1 Structural Properties

Full-Heusler alloys have two possibilities to crystalize first in the $L2_1$ with Cu_2MnAl prototype (space group: $Fm\bar{3}m$ N°:225) or in the XA with Hg_2CuTi prototype (space group: $F\bar{4}3m$ N°:216) structure. Four interpenetrating fcc sub-lattices make up the cubic $L2_1$ structure. *X* atoms occupy two of them at Wyckoff position 8c (0.25, 0.25, 0.25), while *Y* and *Z* atoms occupy the other two at places 4b (0.5, 0.5, 0.5) and 4a (0, 0, 0), respectively. However, it was employed in all four locations for the XA structure: 4a (0, 0, 0), 4b (0.25, 0.25, 0.25), 4c (0.5, 0.5, 0.5), and 4d (0.5, 0.5, 0.5) (0.75, 0.75, 0.75). Mn atoms occupy sites B (0.25, 0.25, 0.25) and D (0.75, 0.75, 0.75) in the $L2_1$ structure, while Hf/Si-Ge atoms occupy sites C (0.5, 0.5, 0.5) and A (0, 0, 0), respectively (Table 1). Together, inequivalent Mn atoms (as named Mn_1/Mn_2) occupy A (0, 0, 0) and B (0.25, 0.25, 0.25), while Hf/Si-Ge occupy C (0.5, 0.5, 0.5) and D (0.75, 0.75, 0.75) sites in the XA structure (see Fig. 1).

First, we study the structural stability to find the most stable geometry because all the physical parameters depend on its crystal structure. It is best characterized for use in the industry based on experimental studies that validate what we found in the calculation. Since the Hf atom is less electronegative than Mn and Hafnium has fewer valence electrons than manganese atoms, the $L2_1$ $AlCu_2Mn$-type structure is projected to be more advantageous than the XA Hg_2CuTi-type structure for the two compounds Mn_2HfSi and Mn_2HfGe. In 5d transition metals, it has been discovered that elements with more valence electrons are more likely to occupy the Wyckoff position 8c (0.25, 0.25, 0.25) in the L21 structure. In contrast, those with less are more likely to occupy 4b (0.5, 0.5, 0.5) and 4a (0, 0, 0), respectively. In both Cu_2MnAl- and Hg_2CuTi-type structures of the full-Heusler alloys Mn_2HfSi and Mn_2HfGe, we estimated the total energy as a function of the cell volume per formula unit for the nonmagnetic (NM) and ferromagnetic (FM) states (see Fig. 2a–b).

Secondly, we notice that our results concern the magnetic stability for the Mn_2HfX since X = Si-Ge. The results show that the FM phases have lower energies than the NM phases in these systems, according to our findings. As a result, Mn atoms prefer to occupy the C sites, whereas Hf and Si-Ge atoms prefer to occupy the B sites and A sites, respectively.

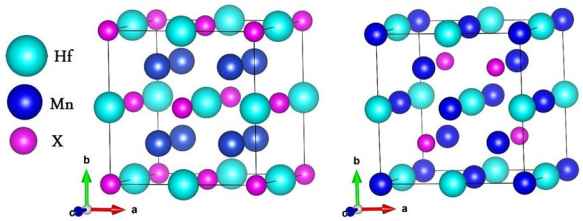

Fig. 1 Regular structures $L2_1$ with Cu_2MnAl prototype and XA with Hg_2CuTi prototype for Mn_2HfX (X = Si, Ge)

By fitting the total energy as a function of volume to the Birch-Murnaghan equation of state, the equilibrium lattice constants a_0, bulk modulus B, and its pressure derivative B are achieved [39]. The projected results are shown in Table 2. Mn_2HfSi and Mn_2HfGe have equilibrium lattice constants of 5.9853 Å and 6.0685 Å, respectively, in $L2_1$ $AlCu_2Mn$-type. Due to the lower atomic radius of Si than that of Ge, the estimated lattice constant of Mn_2HfSi is less than that of Mn_2HfGe. There are no experimental or theoretical data available for comparison to our knowledge.

3.1.2 Thermodynamic Properties

Third, two energy parameters—cohesive energy and formation enthalpy—are used to evaluate the chemical and thermodynamic stabilities of all the compounds. To ascertain chemical stability and investigate if it is possible to create these half-metals in the experiment, these two energy values are defined in Eqs. (1) and (2):

$$E_{coh}\left(Mn_2HfX\right) = \left(E_{total}^{Mn_2HfX} - 2 \times E_{iso}(Mn) - E_{iso}(Hf) - E_{iso}(X)\right) \quad (1)$$

$$\Delta H_r\left(Mn_2HfX\right) = \left(E_{coh}\left(Mn_2HfX\right) - 2E_{coh}(Mn) - E_{coh}(Hf) - E_{coh}(X)\right) \quad (2)$$

We start by the cohesive energy E_{coh}, where E_{total} refers to the total energy of Mn_2HfX since the X = Si-Ge compound of one formula unit at equilibrium volume, and E_{iso}(Mn), E_{iso}(Hf), and $E_{iso}(X)$ are the total energy of isolated atoms. ΔHr (Mn_2HfX) is the formation enthalpy of Mn_2HfX since X = Si-Ge compound; E_{coh}(Mn_2HfX) is the cohesive energy

Table 1 Structural order of regular $L2_1$ (Cu_2MnAl) and inverse XA (Hg_2CuTi) types for the Mn_2HfX (X = Si, Ge), where *A*, *B*, *C* and *D* are the available Wyckoff sites: (0, 0, 0), (0.25, 0.25, 0.25), (0.5, 0.5, 0.5), and (0.75, 0.75, 0.75), respectively

Mn_2HfX (X = Si, Ge)	A (0,0,0)	B (0.25,0.25,0.25)	C (0.5,0.5,0.5)	D (0.75,0.75,0.75)
$L2_1$	Si-Ge	Mn	Hf	Mn
XA	Mn	Hf	Mn	Si-Ge

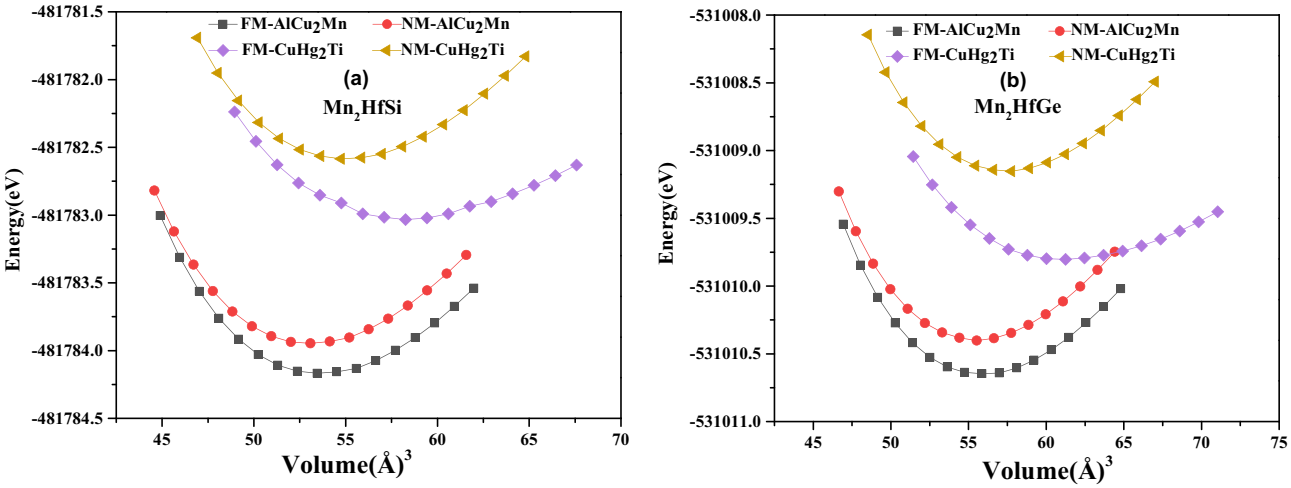

Fig. 2 The total energies as a function of unit cell volumes in the two magnetic phases (FM and NM) in regular structures $L2_1$ with the Cu_2MnAl prototype and XA with the Hg_2CuTi prototype using the GGA approach. **a** Mn_2HfSi and **b** Mn_2HfGe

of Mn_2HfX since X = Si-Ge per formula; E_{coh}(Mn), E_{coh}(Hf), and E_{coh}(X) are the cohesive energy of Mn, Hf, and X = (Si and Ge). The calculated cohesion energy and formation enthalpy of all the compounds in the cubic phase are given in Table 3. The negative values of E_{coh}(Mn_2HfX) and ΔHr (Mn_2HfX) ensure the chemical and thermodynamic stability of Mn_2HfX since X = Si-Ge compounds. As a result, these compounds, Mn_2HfSi and Mn_2HfGe, could be synthesized experimentally.

3.2 Electronic Properties

3.2.1 Band Structure and Density of States

In the $AlCu_2Mn$-type compounds Mn_2HfSi and Mn_2HfGe, we provide the spin-polarized band structures at equilibrium lattice constants in the $L2_1$ phase, along the high-symmetry directions of the first Brillouin zone. To predict the band gap results with more accuracy with the experimental, GGA + U and TB-mBJ are well positioned. The researchers' investigation revealed that GGA-mBJ functional possesses similar accuracy to GGA + U, with small detail's differences [40, 41]. For this reason, our study is focused on GGA-mBJ methods.

We agree with some studies [42, 43] that spin–orbit coupling (SOC) can be of crucial importance for the half-metallic property of some 3d materials, and also, 2d materials are affected by the SOC [44, 45]. For Heusler alloys, the spin–orbit coupling can induce states within the gap, but the alloys keep a very high degree of spin polarization at the Fermi level. Galanakis et al. [46] confirm in their calculation of spin (m_{spin}) and orbital (m_{orb}) magnetic moments for some half- and full-Heusler compounds that the orbital moments in Heusler alloys are expected to be small. For this reason, this study has not considered the effect of spin–orbit coupling (SOC).

It is obviously apparent in Fig. 3a–c. The majority-spin channel has an energy gap G_{Maj} at the Fermi level (E_F), suggesting semiconducting property, as opposed to the minority-spin channel, which is metallic and has intersections at the Fermi level (E_F) (Fig. 3b–d). The band structures of the two materials are similar, as can be seen for these compounds. The indirect band gaps for Mn_2HfSi and Mn_2HfGe, respectively, are 0.689 eV and 0.520 eV at approximately E_F along

Table 2 Equilibrium lattice constant a, bulk modulus B, its derivative B', and the total energy E for Mn_2HfSi and Mn_2HfGe in $L2_1$ and XA structures

		a_0 (Å)	V(Å)^3	B (GPa)	(B′)	E (in eV)
Mn_2HfSi	**L_{21}-FM**	**5.9853**	**214.42**	**196.2877**	**4.2121**	**−481784.17194**
	L_{21}-NM	5.9664	212.39	199.1557	4.2167	−481783.95067
	XA-FM	6.1542	233.08	115.8988	5.5200	−481783.01936
	XA-NM	6.0363	219.94	184.6276	4.1945	−481782.58664
Mn_2HfGe	**L_{21}-FM**	**6.0685**	**223.48**	**183.6331**	**4.4116**	**−531010.65182**
	L_{21}-NM	6.0547	221.96	186.7927	4.2284	−531010.39771
	XA-FM	6.2596	245.27	102.4922	5.9220	−531009.80465
	XA-NM	6.1254	229.83	174.1128	4.3875	−531009.15084

Table 3 Cohesive energy (E_{coh}) and formation enthalpy ΔH_r calculated by GGA, in the most stable magnetic phase $L2_1$, for both compounds Mn_2HfX (X = Si, Ge)

Structure	System energy (eV)	E_{coh} (eV/atom)	ΔH_r (eV/atom)
Mn_2HfSi	−481784.17194	−7.86440	−0.64204
Mn_2HfGe	−531010.65182	−7.49017	−0.44163

the G-X symmetry, according to Fig. 3a–c, in the majority-spin channel. These gaps result in an equilibrium-state HM character due to 100% spin polarization at E_F caused by these gaps. Additionally, we can observe that each compound's spin-up and spin-down band structures are not superposed, indicating that they are magnetic, with a value determined by the difference between the spin-up and the spin-down densities (see the density of state).

In both majority- and minority-spin channels, it is noteworthy that, as shown in Fig. 3a–c, three energy bands of p electrons from Si or Ge atoms cover the majority of the energy region between −6.2 and −3.8 eV. The s band is well separated from other bands and has a very low energy level, so we do not display it. The Si (Ge) s and p electronic states that give rise to the low-lying bands have the same characteristics in both directions. Si (Ge) atoms give s-p states that may be hybridized with transition metal d electrons to control how occupied the p-d orbitals are. This hybridization affects on the energy gap's breadth.

According to Galanakis et al. [12], hybridization occurs in the $L2_1$ structure, between the Mn 3d orbitals and their second nearest neighbors, Mn 3d orbitals, and between the Mn 3d orbitals and their first nearest neighbors, Hf 5d orbitals or Si (Ge) sp states; the hybridization between these atoms is qualitatively very important. The five d orbitals are divided into two doubly degenerate states, d4 and d5 (z^2, x^2-y^2), and three triply degenerate states, d1, d2, and d3 (xy, yz, zx) (Fig. 5a). The e_g orbitals (the t_{2g} orbitals) can only couples with the e_g orbitals (the t_{2g} orbitals) of the other Mn atom forming bonding hybrids, denoted by e_g (or t_{2g}) and antibonding orbitals, denoted by e_u (or t_{1u}).

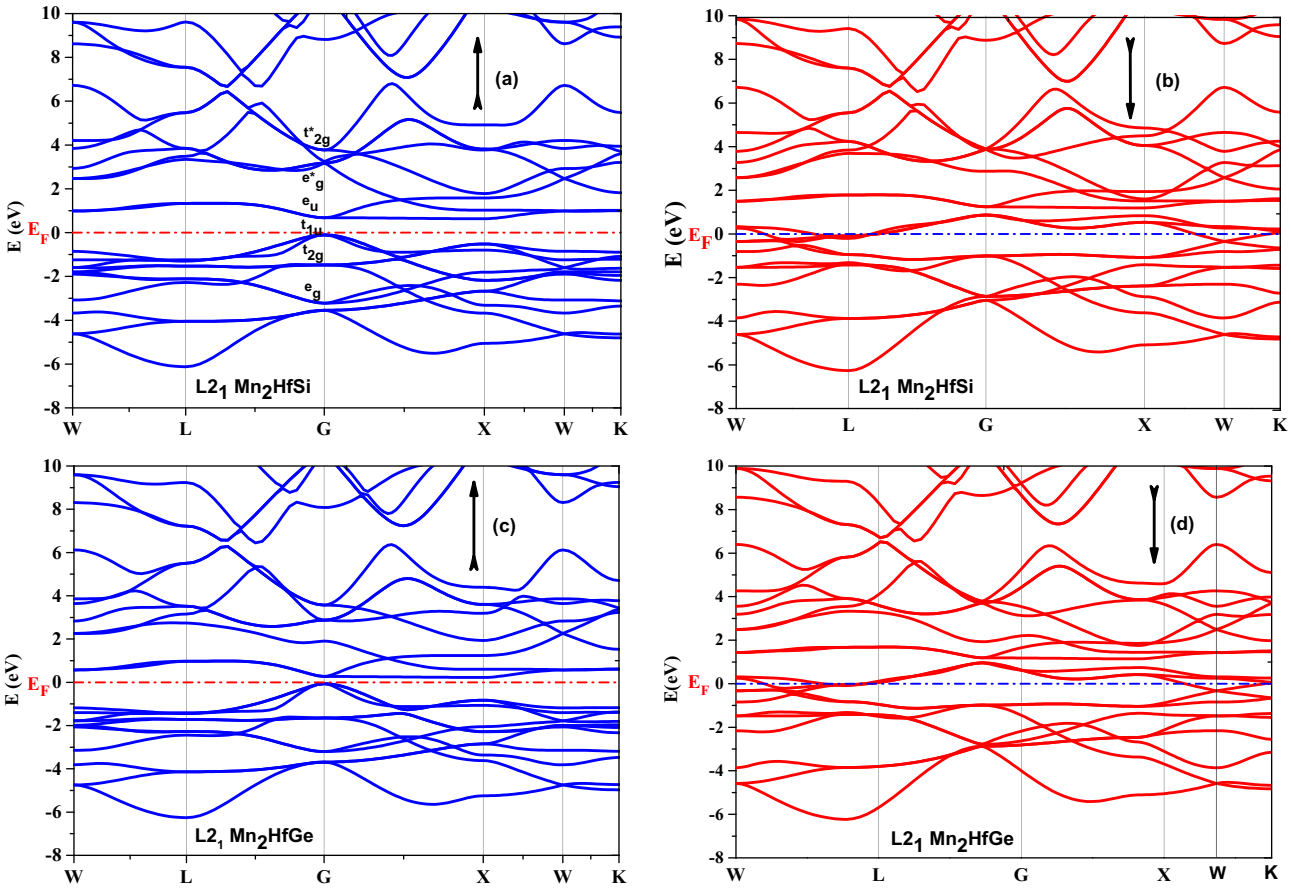

Fig. 3 The calculated GGA-mBJ band structures spin-polarized along the principal high-symmetry directions in the Brillouin zone for the FM phase $L2_1$- Mn_2HfX (X = Si, Ge) at their predicted equilibrium lattice constants: **a** and **b** spin-up and down of Mn_2HfSi. **c** and **d** Spin-up and down of Mn_2HfGe

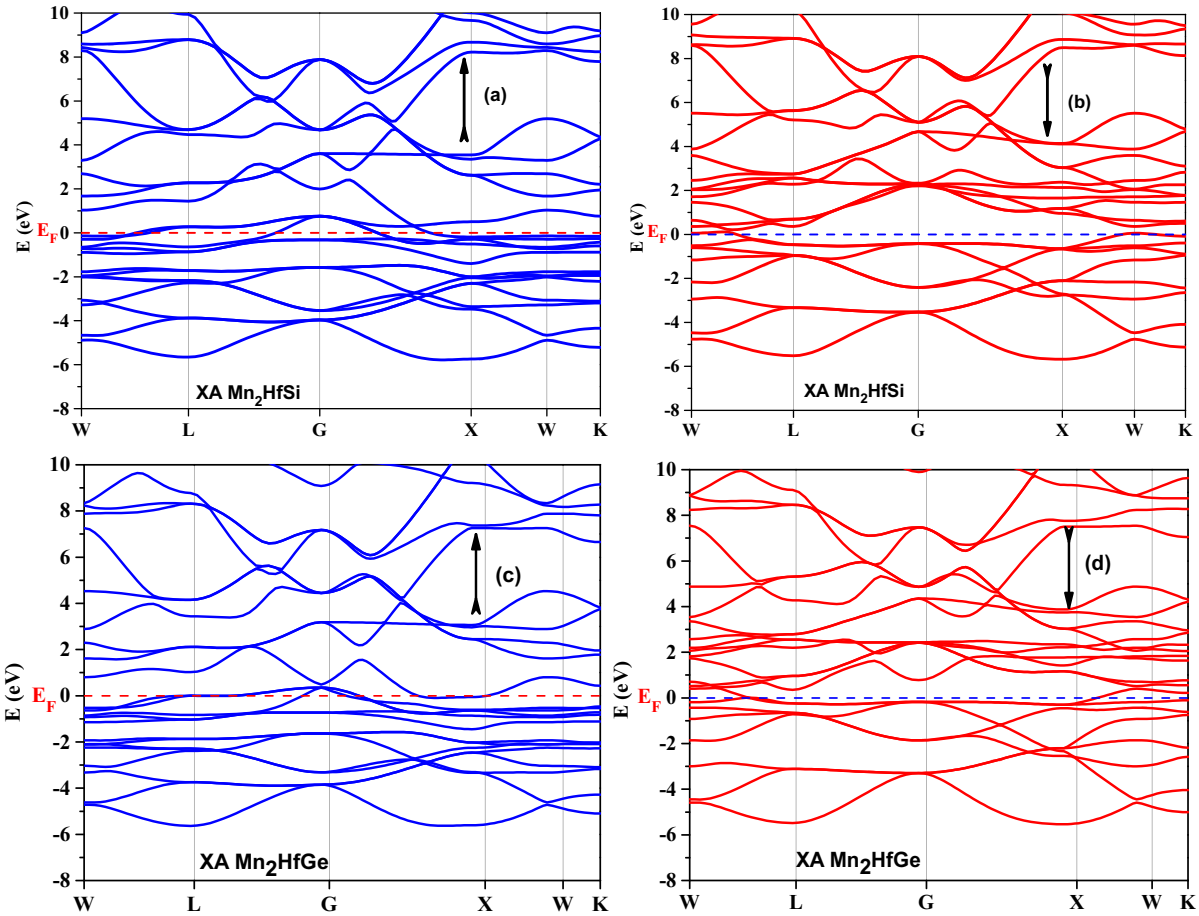

Fig. 4 The calculated GGA-mBJ band structures Spin-polarized along the principal high-symmetry directions in the Brillouin zone for the FM phase XA- Mn_2HfX (X = Si, Ge) at their predicted equilibrium lattice constants: **a** and **b** spin-up and down of Mn_2HfSi. **c** and **d** Spin-up and down of Mn_2HfGe

In the second step, we consider the hybridization of the Mn–Mn orbitals with the d orbitals of Hf (Fig. 5b). The doubly degenerate e_g orbitals hybridize with the d4 and d5 orbitals of Hf, which transform according to the same irreducible representation of the symmetry group. They create doubly degenerate bonding states (e_g), which are very low in energy, and antibonding states unoccupied above the Fermi level. The $3t_{2g}$ orbitals of Mn couple with d1, d2, and d3 of Hf create six new orbitals, of which three are bonding, and the other three are high energy antibonding. Finally, the two e_u and three t_{1u} orbitals of Mn cannot couples with any of the d orbitals of Hf since these do not transform with the u representations, and they are orthogonal to the e_u and t_{1u} states of Mn.

Therefore, these states are antibonding concerning the Hf atoms and the Si (or Ge) atoms. The t_{1u} states are occupied below the Fermi level, while the e_u states are just above the Fermi level. The absence of hybridization between the e_u and t_{1u} states of Mn and the d orbitals of the Hf atoms will result in splitting. The energy gap in the majority spin states is attributed to this $e_u - t_{1u}$ difference. Thus, there are eight filled minority d bands.

To further demonstrate the nature of electronic structures, as a function of energy for the lattice constant of Mn_2HfSi and Mn_2HfGe, and understand the band structure, we have shown the spin-polarized band structures, total density of states (TDOS), and the partial density of states (PDOS) of 3d-Mn, 5d-Hf, and 3p-Si and Ge. According to the approximations of GGA-mBJ as shown in Fig. 6a–b, we have also represented the variation of deg-Mn, dt_{2g}-Mn, d_{eg}-Hf, and dt_{2g}-Hf; where the e_g states have lower energies than the t_{2g} states in the two compounds. The dashed line represents the Fermi level.

From Fig. 6a and b, the partial DOSs of the 3d orbitals of Mn for the two materials show the same behavior. One can also notice that the DOS around and below E_F is mainly associated with the 3d states of Mn, which confirms that the bonding states come mostly from the transition metal of higher valence (the Mn atom), while the partial DOSs of the 5d orbitals of Hf is mostly found above the Fermi level, i.e., the unoccupied antibonding bands are due mainly to the

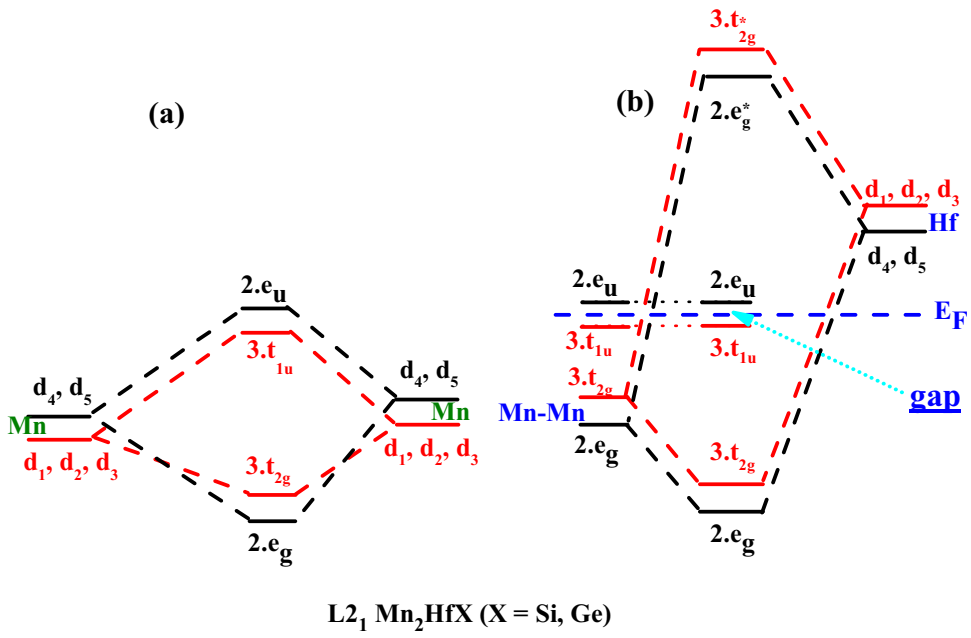

Fig. 5 Schematic diagram at equilibrium lattice constant of possible d–d hybridization spin-up band structures in the Mn_2HfX (X = Si, Ge) alloy, between the transition-metal elements **a** Mn-3d -Mn—3d and **b** Hf-5d—Mn-3d

lower valence transition metal (the Hf atom) [13]. According to the partial DOSs, we notice that the gap, at the Fermi level, between the Hf atoms and the sp atoms is somewhat larger than that of the Mn atom. The peaks above E_F are due to the t_{2g} states. The actual gap is determined by the Mn–Mn interaction or, more precisely, by the $t_{1u} - e_u$ splitting. This also explains why the gaps are relatively small for the Mn_2HfSi and Mn_2HfGe compounds (Table 4).

It is clear that the majority states in these alloys have no DOS at E_F, but the minority states have crossings at the Fermi level, indicating that Mn_2HfSi and Mn_2HfGe compounds are real HMFIs. The range of energy from − 6 to − 3 eV is related to the p bands of the Si or Ge atoms, as seen in Fig. 6a–b. As can be seen, the partial DOSs of Mn 3d orbitals in the two materials exhibit similar conformation. We see that the bonding states predominately reside at the higher valence transition metal Mn atom and that the DOS around and below E_F is connected mainly with the Mn 3d states.

In the inverse XA (Hg_2CuTi) types for Mn_2HfX (X = Si, Ge) (Fig. 4a-d), we have shown the the spin-polarized band structures total density of states (TDOS) and the partial density of states (PDOS) of 3d-Mn, 5d-Hf, and 3p-Si and Ge according to the approximations mBJ-GGA Fig. 7a–b. According to the last figure, it is clear that the metallic behavior in the two channels of spin has intersections at the Fermi level (E_F) in two directions, even though the total magnetic moment per cell remains approximately integer (see Table 4). According to the density morphological results, the electronic structures depend on the atoms' $L2_1$ and XA ordering rather than the GGA or GGA-mBJ method.

3.3 Magnetic Properties

At the equilibrium lattice constants of two compounds, the calculated total magnetic moment is 2.00 μ_B per unit cell. The HM character of these alloys is revealed by the integer value of the magnetic moment. For Mn_2HfSi and Mn_2HfGe, Table 4 displays the computed total, atom-resolved magnetic moments, to which is the contribution of the interstitial regions in the unit cell (interstitial moments).

The Mn atoms contribute the majority of the overall magnetic moment. The significant exchange splitting between the majority and minority spin states of the Mn atom is to blame for this. We also observed that the Hf and sp atoms' partial moments were anti-parallel to the Mn moments in two systems, which results in the ferrimagnetic character.

It is recalled that for full-Heusler alloys, the total magnetic moment of spin satisfies rule 24, which is the analog of the Slater-Pauling rule. In this rule, the total magnetic moment M_{tot}, per formula unit, is related to the total number Z_{tot} of valence electrons in the unit cell by:

$$M_{tot} = \left(Z_{tot} - 24\right)\mu_B. \tag{3}$$

However, for half-metallic in full-Heusler alloys with less than 24 electrons per unit cell, such as the alloys studied in this work, the energy gap is in the majority spin band and not in the minority spin band. In this case, the Slater-Pauling role given by Eq. (3) has been generalized by Skaftouros et al. for inverse Heusler alloys [15], even for

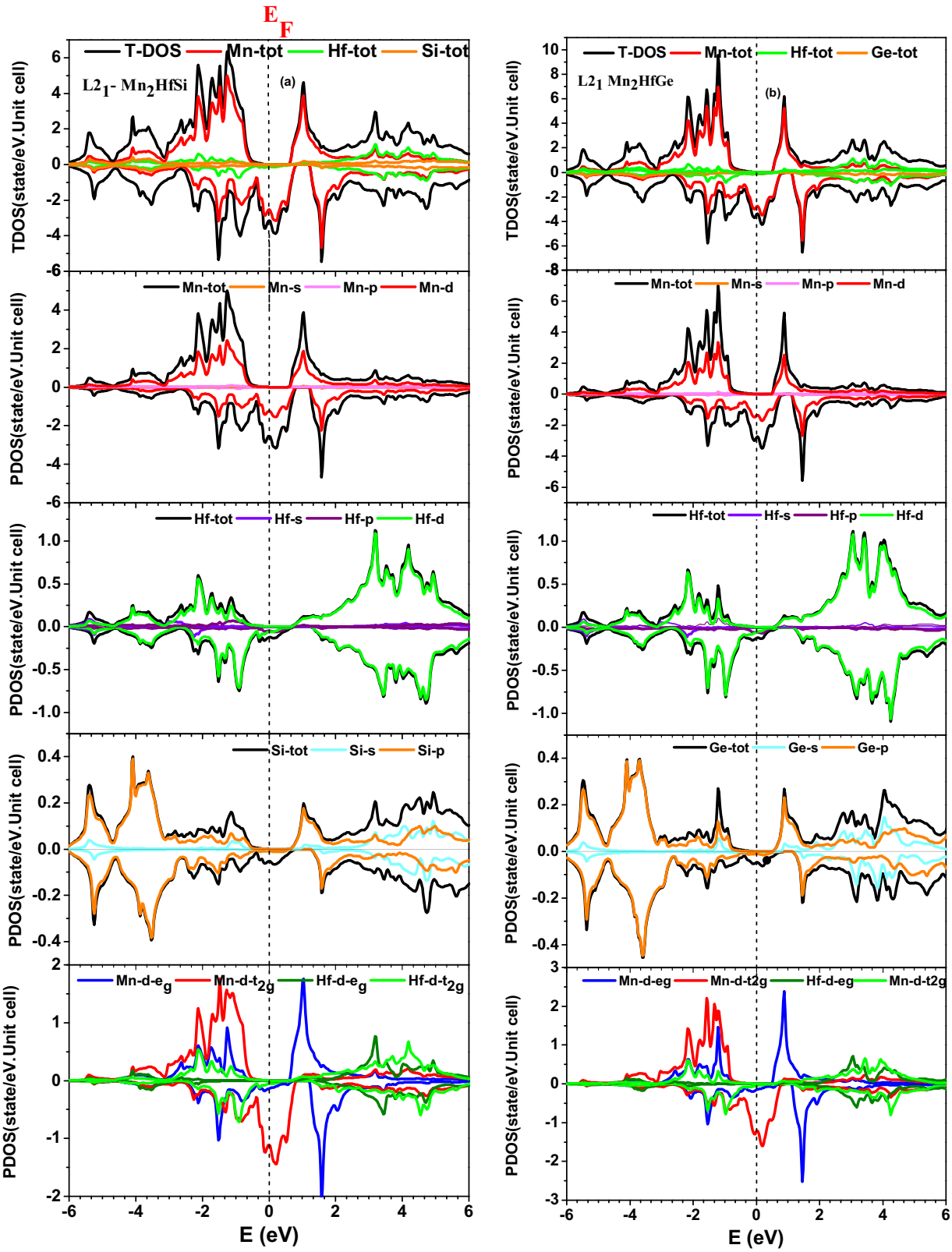

Fig. 6 Spin-up and spin-down total and partial densities of states for the cubic-Mn_2HfX (X = Si, Ge) compound in the $L2_1$- FM phase calculated by GGA-mBJ approach. **a** Mn_2HfSi and **b** Mn_2HfGe

Table 4 The calculated magnetic moments in the unit of (μ_B), the Mn atom moment (M_{Mn}), the Hf atom moment (M_{Hf}), the Si atom moment (M_{Si}), the interstitial moment (M_{int}), and the unit cell total magnetic moment (M_{tot}) for Mn_2HfSi and Mn_2HfGe

		M_{Mn1}	M_{Mn2}	M_{Hf}	M_{Si}	$\mathbf{M_{Tot}}$	M_{int}
Mn_2HSi	**$L2_1$- GGA**	1.102	–	−0.138	−0.045	1.999	−0.019
	$L2_1$- GGA-mBJ	1.123	–	−0.162	−0.050	2.000	−0.034
	XA- GGA	2.011	1.882	0.006	−0.040	3.988	0.128
	XA- GGA-mBJ	2.269	1.915	−0.030	−0.057	4.166	0.068
Mn_2HGe	**L_{21}- GGA**	1.129	–	−0.169	−0.042	2	−0.047
	L_{21}- GGA-mBJ	1.173	–	−0.211	−0.05	2	−0.085
	XA- GGA	2.782	2.328	−0.01	−0.041	5.04	0.072
	XA- GGA-mBJ	2.875	2.319	−0.116	−0.052	5.036	0.01

full-Heusler alloys containing less than 24 electrons, such as Mn_2ZrSi and Mn_2ZrGe [16]. Therefore, the appropriate (adequate) Slater-Pauling rule for Mn_2HfSi and Mn_2HfGe is $M_{tot} = Z_{tot} - 24$.

Indeed, the total spin magnetic moment M_{tot} is just the number of uncompensated spin magnetic moments, so:

$$M_{tot} = \left(Z_{maj} - Z_{min}\right)\mu_B = (2Z_{maj} - Z_{tot})\mu_B \quad (4)$$

Z_{maj} and Z_{min} are the numbers of occupied majority and minority spin states, respectively, with $Z_{tot} = Z_{maj} + Z_{min}$. In both, Mn_2HfSi and Mn_2HfGe, the majority-spin bands are occupied by a total of twelve electrons per unit cell [47, 48]: 1 s, 3p, 2, $3t_{2g}$, and $3t_{1u}$ (see Fig. 3a–c). Then, with Z_{maj}, the appropriate relation for such compounds is:

$$M_{tot} = (24 - Z_{tot})\mu_B \quad (5)$$

According to this rule, the total magnetic moment of Mn_2HfSi and Mn_2HfGe alloys with 22 valence electrons should be around 2.00 μ_B. Abada et al. derived the same relationship for Mn_2ZrZ (Z = Si, Ge) [16].

Calculations were approved for lattice parameters ranging from 5.6 to 6.3 Å for this determination in phase $L2_1$. Figure 8a–b shows the half-metallicity character above the constant lattice values of 5.98 Å and 6.07 Å for Mn_2HfSi and Mn_2HfGe, respectively. Ferrimagnetic behavior results in both compounds over 5.7–6.2 for Mn_2HfSi and 5.75–6.2 for Mn_2HfGe. The total magnetic moments for both compounds have integer values. The atoms of Mn have positive magnetic moments, while the two atoms of Hf and Si-Ge have negative magnetic moments. In addition, our compounds have a significant area of half-metallicity, due to their stability at both positive and negative pressures. When the lattice constants are modified in this interval, as we mentioned before, Mn_2HfSi and Mn_2HfGe keep their half-metallicity. This study demonstrates that the half-metallicity is more stable in constant lattice fluctuation.

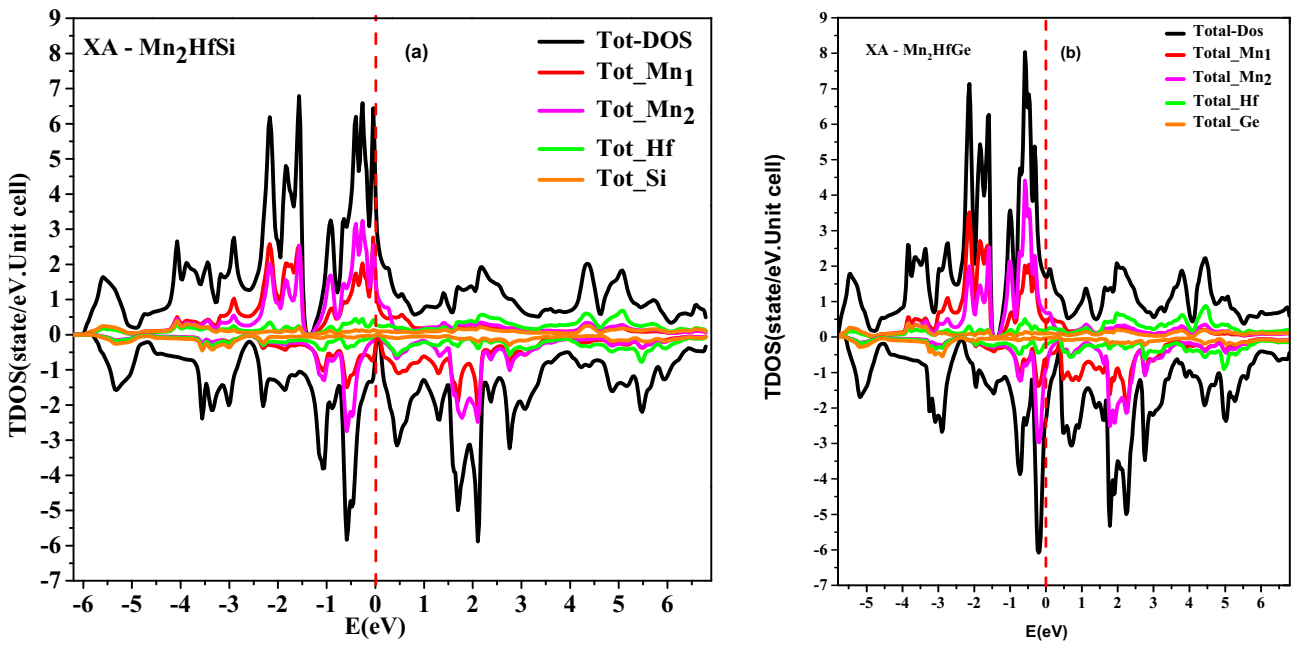

Fig. 7 Spin-up and spin-down total and partial densities of states for the cubic-Mn_2HfX (X = Si, Ge) compound in the XA- FM phase calculated by GGA-mBJ approach. The left panel Mn_2HfSi and the right panel Mn_2HfGe

Table 5 The calculated elastic constants Cij (in GPa), bulk, Young's, and shear modulus (in GPa), the anisotropy factor (A), Cauchy pressure (CP), Pugh's ratio (B/G), Poisson's ratio (ν), and Debye temperature θ_D (K) for Mn_2HfX (X = Si, Ge) in $L2_1$ phase

	Mn_2HfSi	Mn_2HfGe
C_{11}	314.46	224.80
C_{12}	170.19	116.67
C_{44}	86.65	53.67
C_{11}-C_{12}	144.24	108.13
$C_{11}+2C_{12}$	654.84	458.14
B	218.28	152.71
A	1.20	0.83
CP	83.54	63.67
E	215.19	154.26
G	80.55	57.62
B/G	2.71	2.76
υ	0.335	0.34
θ_D	425.34	379.823

Table 4 shows no difference in the magnetic moment between the two mentioned approximations: GGA-mBJ and GGA-PBE, and they give identical values of 2.00 μ_B. This integer number ($M_{tot} = 2\,\mu_B$) for total magnetic moment confirms that Mn_2HfSi and Mn_2HfGe compounds follow the Slater-Pauling rule $M_{tot} = Z_{tot} - 24$ [49, 50]. Furthermore, our full-Heusler alloys Mn_2HfSi and Mn_2HfGe are distinguished by 100% spin polarization at the Fermi level, as determined by a simple calculation based on the polarization rule [51]:

$$p = \frac{n\uparrow(E_F) - n\downarrow(E_F)}{n\uparrow(E_F) + n\downarrow(E_F)} \times 100 \tag{6}$$

where $n\uparrow(E_F)$ and $n\downarrow(E_F)$ are the state densities for spins up and down, and before all this, they exhibit a half-metallicity (see Fig. 6a–b). All these results reveal that these compounds are potential materials for spintronic applications. We can see that Mn contributes the majority of the overall magnetic moment, while interstitial magnetic moments (M_{inter}) and sp element (M_X) are neglected.

3.4 Mechanical Properties

3.4.1 Elastic Properties

We studied the mechanical stability of the alloys Mn_2HfSi and Mn_2HfGe to confirm this stability by calculating the elastic constants, which describe many features such as the crystal's response to applied forces, mechanical properties, structural stability, anisotropy, and bond indexes of solids. The elastic constants for cubic structures are simplified to three independent constants, C_{11}, C_{12}, and C_{44} because of the symmetry of this system. Due to this system's symmetry and for cubic structures, the elastic constants C_{11}, C_{12}, and C_{44} are simplified to three independent constants. So we have calculated the elastic constants C_{11}, C_{12}, and C_{44} by fitting the total energy of the strained crystal. The results obtained are given in Table 5. The determined elastic constants in the $L2_1$ phase are favorable and support the stability criterion, demonstrating the mechanical stability of the two compounds, Mn_2HfSi and Mn_2HfGe:

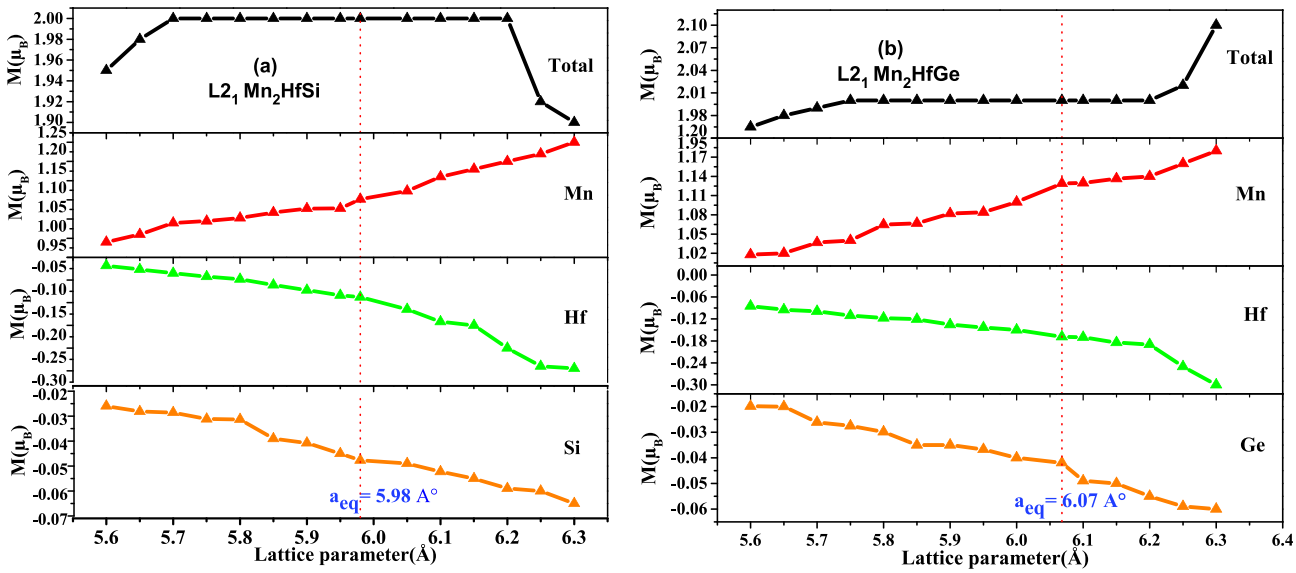

Fig. 8 The calculated total and partial magnetic moment of Mn, Hf, and the sp element as functions of lattice constant: **a** Mn_2HfSi and **b** Mn_2HfGe. The dotted lines indicate the equilibrium lattice constants

$$C_{11} > 0;\ C_{12} > 0;\ C_{44} > 0;\ C_{11} - C_{12} > 0;\ C_{11} + 2C_{12} > 0;\ C_{11} > B > C_{12}. \tag{7}$$

Phase $L2_1$ (see Table 5) shows the results collected until now.

The structures of Mn_2HfSi and Mn_2HfGe have positive values for the Cauchy pressure (CP), defined as the difference between C_{12} and C_{44} that indicates a ductile nature, while the negative value indicates brittleness. Additionally, the material is described as ductile if the Pugh's ratio (PR), also known as the B/G ratio, is larger than 1.75 and brittle if the PR is lower than 1.75. [52]. Our PR value demonstrates that Mn_2HfSi and Mn_2HfGe are ductile. Furthermore, the Poisson ratio (υ) confirmed these conclusions. Brittle materials have a value of $\upsilon < 0.26$, while ductile materials have a value of $\upsilon > 0.26$ [53].

3.4.2 Polycrystalline Elastic Moduli

The terms "bulk modulus," "shear modulus," and "Young's modulus" indicate the materials' resistance to volume change, their tolerance for shape change, and their stiffness, respectively.

We employed the widely known Voigt-Reuss-Hill (VRH) [54]. The isotropic bulk modulus B and the shear modulus G are defined as follows in this approximation:

$$B = B_V = B_R = (C_{11} + 2C_{12})/3 \tag{8}$$

$$G = (G_V + G_R)/2 \tag{9}$$

$$G_V = (C_{11} - C_{12} + 3C_{44})/5 \tag{10}$$

$$G_R = 5C_{44}(C_{11} - C_{12})/(4C_{44} + 3(C_{11} - C_{12})) \tag{11}$$

$$E = 9BG/(3B + G) \tag{12}$$

$$A = 2C_{44}/(C_{11} - C_{12}) \tag{13}$$

$$CP = C_{12} - C_{44} \tag{14}$$

$$v = (3B - 2G)/2(3B + G) \tag{15}$$

where V and R subscript denotes Voigt and Reuss bound, respectively.

Young's modulus is a mathematical term that refers to the modulus of the ratio of linear stress to strain, which is defined as E.

A material with a high B and G value implies a high resistance to the relevant changes, but a stiffer material has a higher E value.

For both compounds, the shear modulus G is lower than the bulk modulus B; therefore, we deduce that they are more resistive to hydrostatic pressure than shear. Young's E and shear modulus G of Mn_2HfSi are larger than Mn_2HfGe, so Mn_2HfSi is more tensile (stiffer) than Mn_2HfGe. Furthermore, a perfect isotropic material has an anisotropic factor $A = 1$, but any other value of A causes the material to be anisotropic. As a result, the Zener anisotropy factor A is 1.20 for Mn_2HfSi and 0.83 for Mn_2HfGe. Based on these values, our compounds are closer to the isotropic materials.

Our compounds are ductile, as evidenced by the predicted B/G ratios of 2.71 for Mn_2HfSi and 2.76 for Mn_2HfGe. In addition, the alloy Mn_2HfSi displays a CP of 83.54 GPa and 63.67 GPa for Mn_2HfGe. The positive value of this measure validates the alloy's ductility, resulting in an appropriate B/G ratio. Finally, the Poisson's ratio is 0.33 for Mn_2HfSi and 0.34 for Mn_2HfGe. Lewandowski et al. [55] examined a very different class of materials. They concluded that a drastic change in failure behavior correlates with the change in Poisson's ratio, and the apparent signal change occurs somewhere between $\nu = 0.26$ and $\nu = 0.31$. Higher values of ν signal ductility and lower values signify brittle behavior.

So based on this result, the conclusion, demonstrating that our materials have the behavior of metallic ductility in their equilibrium states, this result shows that these two compounds have a promising future in spintronics, especially in terms of the hardness of the slices.

3.4.3 Debye Temperature

The Debye temperature, which is linked to several physical characteristics of solids, including specific heat, elastic constants, and melting temperature, is a crucial metric in the study of material properties. A more considerable Debye temperature means a bigger bonding strength, and vice versa [56]. From Table 5, one can note that the studied compounds Mn_2HfX (X = Si, Ge) possess a relatively low Debye temperature (Figs. 9 and 10). At low temperatures (below Θ_D), when $T < \Theta_D$, only low-frequency vibrations are excited [57, 58]. That is what we can see in the phonon dispersion curves (Fig. 11a–b), whereas at higher temperatures (above Θ_D), the movement is more disordered, and all vibration modes are excited.

Based on the calculated density and elastic constants data, we can calculate the Debye temperature Θ_D using the following formula [59]:

$$\Theta_D = \frac{h}{k}\left[\frac{3n}{4\pi}\left(\frac{N_A\rho}{M}\right)\right]^{1/3} v_m \tag{16}$$

h is the Planck constant, k is Boltzmann's constant, n is the number of atoms in the molecule, N_A is the Avogadro

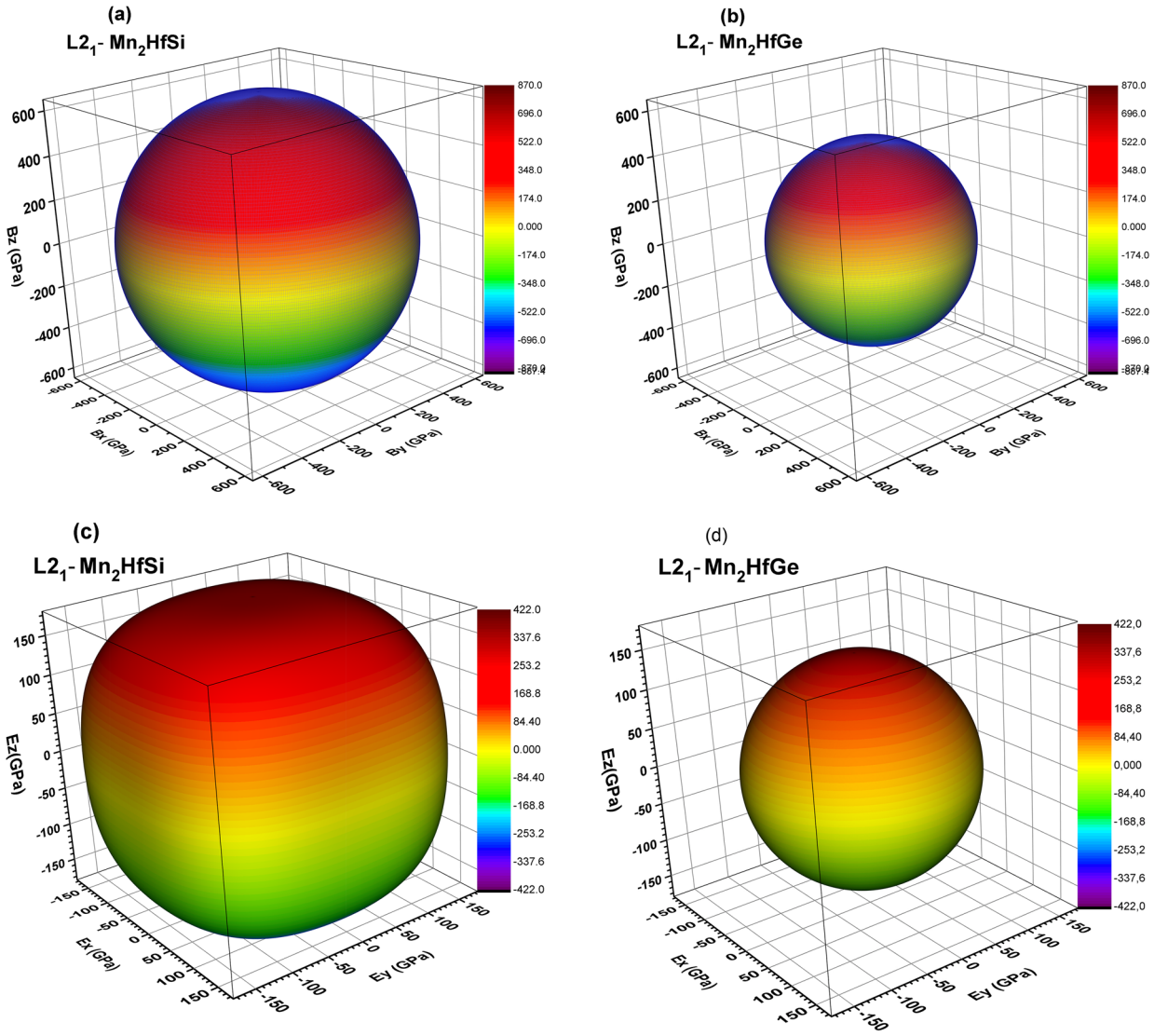

Fig. 9 3D surface expressing the directional dependence: **a** and **c** bulk modulus (B) for Mn_2HfSi; **b** and **d** Young's (E) modulus for Mn_2HfGe

number, ρ is the density, M is the molar mass, and v_m is the average sound velocity, which can be calculated as follows:

$$v_m = \left[\frac{1}{3}\left(\frac{2}{v_t^3} + \frac{1}{v_l^3}\right)\right]^{-1/3} \tag{17}$$

Here, v_t and v_l are the transverse and longitudinal elastic wave velocity, respectively, obtained using the bulk modulus B and the shear modulus G in the following equations:

$$v_t = \left(\frac{G}{\rho}\right)^{1/2} \text{and } v_l = \left(\frac{B + \frac{4}{3}G}{\rho}\right)^{1/2} \tag{18}$$

3.4.4 Anisotropy of Mechanical Behavior

To illustrate the anisotropy of the polycrystalline bulk (B) and Young modulus (E) is to plot them on the two-dimensional surface (and/or three-dimensional) as a function of direction. We plotted Young's (E) and bulk (B) modulus in different directions using spherical coordinates for Mn_2HfX (X = Si, Ge). Regarding the cubic crystal class, the directional dependence of Young modulus (E) and bulk modulus (B) can be expressed as follows [60]:

$$1/B = (S_{11} + 2S_{12})(l_1^2 + l_2^2 + l_3^2) \tag{19}$$

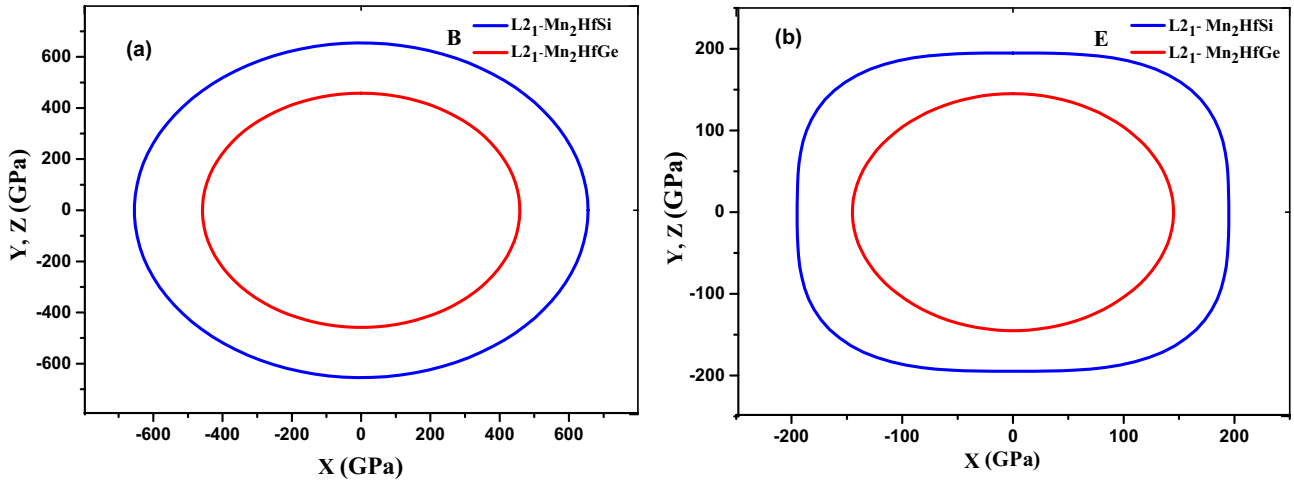

Fig. 10 2D surface expressing the directional dependence of **a** bulk modulus (B) and **b** Young's (E) modulus (in GPa) for Mn_2HfX (X = Si, Ge)

$$\frac{1}{E} = S_{11} - \left(S_{11} - S_{12} - \frac{1}{2}S_{44}\right)(l_1^2 l_2^2 + l_2^2 l_3^2 + l_3^2 l_1^2) \tag{20}$$

In the equations above, Sij represents the compliance matrix, and l_1, l_2, and l_3 are the direction cosines, which are given as $l_1 = \sin\theta\cos\phi$, $l_2 = \sin\theta\sin\phi$, and $l_3 = \cos\theta$ in the spherical coordinates.

2D directional dependence would give rise to a circle shape for an isotropic system, which we see for the bulk and Young modulus in the two compounds Mn_2HfX (X = Si, Ge), except for the Young's modulus for Mn_2HfSi, which present a small degree of anisotropy due to the deviation degree from the circle shape.

Since the system is cubic, the 3D illustration plot and the projections on XY ($XY = XZ = YZ$) planes of the bulk and Young's modulus are shown in Figs. 9a–d and 10a–b. This figure shows that along the X-, Y-, and Z-axis, the compression is the same for all studied compounds. For Young's modulus, we note that the maximum values occur when the stress is applied along the crystallographic bisector direction

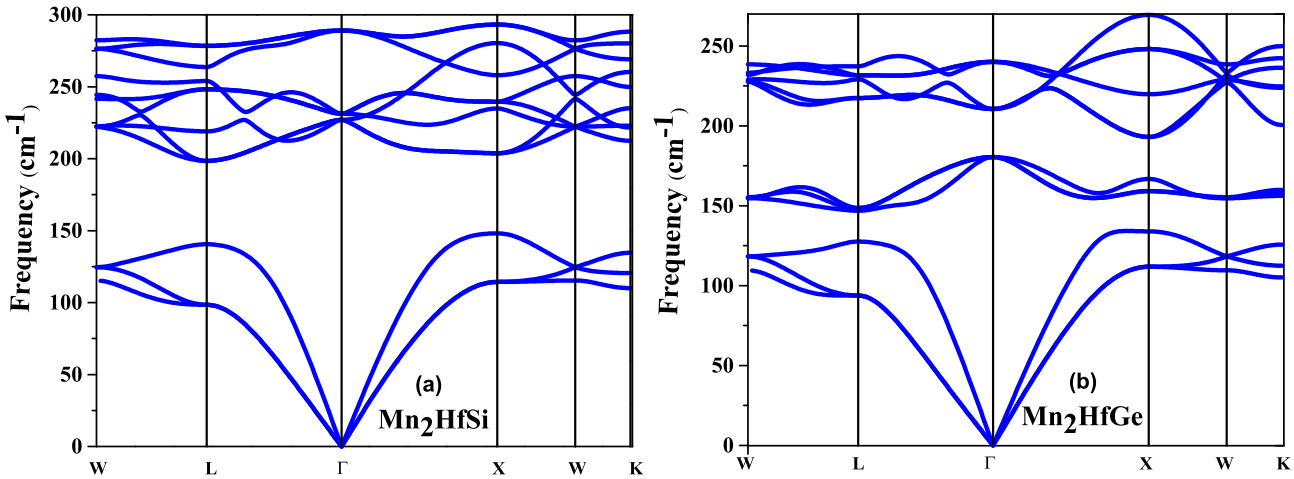

Fig. 11 The phonon dispersion curve for the cubic Mn_2HfX (X = Si and Ge) in the FM state using GGA. **a** Mn_2HfSi and **b** Mn_2HfGe

axe in the XY coordinate plane. In contrast, the minimum values are realized when the stress is applied along the X ($X=Y=Z$) crystallographic axe.

3.5 Dynamical Properties

Finally, to ensure the stability of Mn_2HfX ($X=$ Si and Ge) compounds in the cubic structure $L2_1$- with prototype Cu_2MnAl, we need to compute the dynamic stability through the phonon dispersion curves. So the characteristics of phonons have significant importance in studying crystalline materials; they show the material's response to atomic vibration. Various physical properties of materials can be determined directly or indirectly from the phonon dispersion spectra and phonon DOS [22]. With the help of phonon dispersion spectra (PDS), the structural stability, the phase transition, and the contribution of vibrations in a material's thermal and charge transport properties can be explained [23]. The phonon dispersion curves of Mn_2HfX ($X=$ Si and Ge) in the ground state have been calculated by the pseudo-potential-based Quantum Espresso package within the framework of GGA-PBE [5].

Unlike the supercell method, the approach used to calculate the phonon dispersion is based on linear response theory. This fact is used in the linear response density functional calculations to construct the dynamical matrix using Density-Functional Perturbation Theory (DFPT) [61–69], which gives access to phonon frequency, group velocity, and phonon interaction.

The phonon dispersion curves (PDC) of Mn_2HfX ($X=$ Si and Ge) along the high symmetry directions of the Brillouin zone (BZ) at zero pressure are illustrated in Fig. 11a–b. It can be seen that they are no imaginary modes, which means no negative frequency at the gamma point in PDC. However, the PDC of Mn_2HfX ($X=$ Si and Ge) exhibits positive phonon frequencies in the Brillouin zone's whole region, indicating that the two structures are dynamically stable. The acoustic modes are null at point G in these two compounds and up to 100 cm^{-1} at point W. There is a clear spectral gap between the acoustic and optical phonon branches in the PDC of Mn_2HfX ($X=$ Si and Ge). The formation of this gap is essentially due to the difference in the mass of atoms. Indeed, the phonon vibrational frequencies have a dependence in $\sqrt{\frac{k}{m}}$, k is the force constants, and m is the masses of atoms. The optical phonons of Mn_2HfSi are coupled, on the contrary for Mn_2HfGe. So our materials under investigation are dynamically stable.

4 Conclusion

In conclusion, the first-principles research of the new full-Heusler alloys Mn_2HfSi and Mn_2HfGe was carried out, using GGA and GGA-mBJ in the Density Functional Theory with the code Wien2k. The Cu_2MnAl-type and Hg_2CuTi-type alloys' energies in the NM and FM states were calculated using the $L2_1$ and XA structures, respectively. We discovered that these compounds are stable with a spin polarization of 100% at E_F in the $AlCu_2Mn$-type with $L2_1$ structure. Furthermore, the optimized lattice constants in the ideal structure $L2_1$ for Mn_2HfSi and Mn_2HfGe are predicted to be 5.98 Å and 6.07 Å. Additionally, the partial moments of Hf and Si-Ge atoms in two alloys have negative values. They are anti-parallel to the positive moments of Mn atoms, confirming that our compounds, Mn_2HfSi and Mn_2HfGe, are HMFIs with indirect band gaps that are, respectively, 0.689 eV and 0.520 eV in the majority-spin channel. A total magnetic moment is an integer number of 2.00 μ_B per formula unit, which follows the Slater-Pauling rule of $M_{tot}=Z_{tot}-24$. It is confirmed that there is no change in magnetic moment between the two specified approximations, GGA-mBJ and GGA-PBE. The half-metallicity of these structures is maintained for lattice constants in the range of 5.70–6.20 Å for Mn_2HfSi and 5.75–6.20 Å for Mn_2HfGe, respectively, resulting in stability against constant lattice changes due to the vast half-metallicity area in these compounds. According to the elastic constant calculated anisotropic properties, both materials, Mn_2HfSi and Mn_2HfGe, are almost isotropic.

Author Contribution The authors confirm their contribution to the paper as follows:

Mohamed Lamine Belkhir: conceptualization, data collection and design, and investigation. Ahmed Gueddouh: writing—original draft, supervision, investigation, resources, writing—review and editing, and validation. Fares Faid: supervision and validation. Mourad Rougab: design and investigation.

Data Availability We confirm that we know the research data policy, and the data are available in this paper and on a request from the corresponding author.

Declarations

Competing Interests The authors declare no competing interests.

References

1. Kieven, D., Klenk, R., Naghavi, S., Felser, C., Gruhn, T.: I-II-V half-Heusler compounds for optoelectronics: ab initio calculations. Phys. Rev. B **81**, 075208 (2010)

2. De Boeck, J., Van Roy, W., Das, J., Motsnyi, V., Liu, Z., Lagae, L., Boeve, H., Dessein, K., Borghs, G.: Technology and materials issues in semiconductor-based magnetoelectronics. Semicon. Sci. Technol. **17**, 342 (2002)
3. Kimura, Y., Tamura, Y., Kita, T.: Thermoelectric properties of directionally solidified half-Heusler compound NbCoSn alloys. Appl. Phys. Lett. **92**, 012105 (2008)
4. Jin, Y., Kharel, P., Valloppilly, S., Li, X.-Z., Kim, D., Zhao, G., Chen, T., Choudhary, R., Kashyap, A., Skomski, R.: Half-metallicity in highly L21-ordered CoFeCrAl thin films Appl. Phys. Lett. **109**, 142410 (2016)
5. Wolf, S., Awschalom, D., Buhrman, R., Daughton, J., von Molnár, V.S., Roukes, M., Chtchelkanova, A.Y., Treger, D.: Spintronics: a spin-based electronics vision for the future. Science **294**, 1488–95 (2021)
6. Wang, S., Pratama, F., Ukhtary, M.S., Saito, R.: Independent degrees of freedom in two-dimensional materials. Phys. Rev. B **101**, 081414 (2020)
7. Wang, S.-K., Tian, H.-Y., Yang, Y.-H., Wang, J.: Spin and valley half metal induced by staggered potential and magnetization in silicene. Chin. Phys. B **23**, 017203 (2013)
8. Wang, S., Yu, J.: Magnetic behaviors of 3d transition metal-doped silicane: a first-principle study. J. Superconduct. Nov. Magnet. **31**, 2789–95 (2018)
9. Prinz, G.A.: Magnetoelectron. Sci. **282**, 1660–1663 (1998)
10. Chadov, S., Graf, T., Chadova, K., Dai, X., Casper, F., Fecher, G.H., Felser, C.: Efficient spin injector scheme based on Heusler materials. Phys. Rev. Lett. **107**, 047202 (2011)
11. Faleev, S.V., Ferrante, Y., Jeong, J., Samant, M.G., Jones, B., Parkin, S.S.: Unified explanation of chemical ordering, the Slater-Pauling rule, and half-metallicity in full Heusler compounds. Phys. Rev. B **95**, 045140 (2017)
12. Galanakis, I., Dederichs, P., Papanikolaou, N.: Slater-Pauling behavior and origin of the half-metallicity of the full-Heusler alloys. Phys. Rev. B **66**, 174429 (2002)
13. Galanakis, I., Dederichs, P., Papanikolaou, N.: Origin and properties of the gap in the half-ferromagnetic Heusler alloys. Phys. Rev. B **66**, 134428 (2002)
14. Pickett, W.E., Moodera, J.S.: Half metallic magnets. Physi. Today **54**, 39–45 (2001)
15. Skaftouros, S., Özdoğan, K., Şaşıoğlu, E., Galanakis, I.: Generalized Slater-Pauling rule for the inverse Heusler compounds. Phys. Rev. B **87**, 024420 (2013)
16. Abada, A., Amara, K., Hiadsi, S., Amrani, B.: First principles study of a new half-metallic ferrimagnets Mn2-based full Heusler compounds: Mn2ZrSi and Mn2ZrGe. J. Magnet. Magnetic Mater. **388**, 59–67 (2015)
17. Meinert, M., Schmalhorst, J.-M., Reiss, G.: Ab initio prediction of ferrimagnetism, exchange interactions and Curie temperatures in Mn2TiZ Heusler compounds. J. Phys.: Condens. Matter **23**, 036001 (2010)
18. Gasi, T., Nayak, A.K., Winterlik, J., Ksenofontov, V., Adler, P., Nicklas, M., Felser, C.: Exchange-spring like magnetic behavior of the tetragonal Heusler compound Mn2FeGa as a candidate for spin-transfer torque. Appl. Phys. Lett. **102**, 202402 (2013)
19. Meinert, M., Schmalhorst, J.-M., Reiss, G.: Exchange interactions and Curie temperatures of Mn2CoZ compounds. J. Phys.: Condens. Matter **23**, 116005 (2011)
20. Kubota, T., Kodama, K., Nakamura, T., Sakuraba, Y., Oogane, M., Takanashi, K., Ando, Y.: Ferrimagnetism in epitaxially grown Mn 2 VAl Heusler alloy investigated by means of soft x-ray magnetic circular dichroism. Appl. Phys. Lett. **95**, 222503 (2009)
21. Özdogan, K., Galanakis, I., Şaşioglu, E., Aktaş, B.: Search for half-metallic ferrimagnetism in V-based Heusler alloys Mn2VZ (Z= Al, Ga, In, Si, Ge, Sn). J. Phys.: Condens. Matter **18**, 2905 (2006)
22. Luo, H., Zhu, Z., Liu, G., Xu, S., Wu, G., Liu, H., Qu, J., Li, Y.: Prediction of half-metallic properties for the Heusler alloys Mn2CrZ (Z= Al, Ga, Si, Ge, Sb): a first-principles study. J. Magnet. Magnetic Mater. **320**, 421–8 (2008)
23. Li, S., Ren, Z., Zhang, X., Cao, C.: Electronic structure and magnetism of Mn2CuAl: a first-principles study. Phys. B: Condens. Matter **404**, 1965–8 (2009)
24. Wei, X.-P., Hu, X.-R., Mao, G.-Y., Chu, S.-B., Lei, T., Hu, L.-B., Deng, J.-B.: Half-metallic ferrimagnetism in Mn2CuGe. J. Magnet. Magnetic Mater. **322**, 3204–7 (2010)
25. Liu, L., Hu, L., Liu S., Xiong, J., Liao, Q., Wen, Y.: First-principles investigations on the ground-state bulk properties and lattice constant dependent half-metallic ferrimagnetism of Mn2NbSi full-Heusler compound. Int. J. Quant. Chem. **121**, e26566 (2021)
26. Benaddi, F., Belkharroubi, F., Ramdani, N., Ameri, M., Haouari, S., Ameri, I., Drici, L., Azzi, S., Al-Douri, Y.: Electronic and magnetic investigation of half-metallic ferrimagnetic full-Heusler Mn2IrGe. Emerg. Mater. **4**, 1745–60 (2021)
27. Ram, M., Saxena, A., Aly, A.E., Shankar, A.: Half-metallicity in new Heusler alloys Mn 2 ScZ (Z= Si, Ge, Sn). RSC Adv. **10**, 7661–70 (2020)
28. Ram, M., Saxena, A., Aly, A.E., Shankar, A.: Study of half metallicity, structural and mechanical properties in inverse Heusler alloy Mn 2 ZnSi (1− x) Ge x and a superlattice. RSC Adv. **9**, 36680–9 (2019)
29. Sokolovskiy, V.V., Zagrebin, M.A., Sokolovskaya, Y., Buchelnikov, V.D.: Structural and magnetic properties of Mn2NiZ (Z= Ga, In, Sn, Sb) Heusler alloys from ab initio calculations. In: Solid State Phenomena: Trans Tech Publ) pp 229–32 (2015)
30. Jiang, D., Ye, Y., Yao, W., Zeng, D., Zhou, J., Ruan, W., Wen, Y.: First-principles predictions on half-metallic, mechanical, and acoustic properties of CuHg2Ti-type Mn2LiZ (Z= As, Sb) compounds. J. Superconduct. Nov. Magnet. **33**, 1065–72 (2020)
31. Yousuf, S., Gupta, D.: Robustness in spin polarization and thermoelectricity in newly tailored Mn2-based Heusler alloys. Indian J. Phys. **92**, 855–64 (2018)
32. Wan, H., Yao, W., Zeng, D., Zhou, J., Ruan, W., Liu, L., Wen, Y.: Structural, elastic, electronic, and magnetic properties of a new full-Heusler alloy Mn2MgGe: first-principles calculations. J. Superconduct. Nov. Magnet. **32**, 3001–8 (2019)
33. Maizia, A., Belkharroubi, F., Bourdim, M., Khelfaoui, F., Azzi, S., Amara, K.: First-principles study of a half-metallic ferrimagnetic new full-Heusler Mn2OsGe alloy. In: *Spin*: World Scientific) p 2050026 (2020)
34. Blaha, P., Schwarz, K., Madsen, G.K., Kvasnicka, D., Luitz, J.: wien2k An augmented plane wave+ local orbitals program for calculating crystal properties **60**, (2001)
35. Perdew, J.P., Burke, K., Ernzerhof, M.: Generalized gradient approximation made simple. Phys. Rev. Lett. **77**, 3865 (1996)
36. Perdew, J.P., Burke, K., Wang, Y.: Generalized gradient approximation for the exchange-correlation hole of a many-electron system. Phys. Rev. B **54**, 16533 (1996)
37. Tran, F., Blaha, P.: Accurate band gaps of semiconductors and insulators with a semilocal exchange-correlation potential. Phys. Rev. Lett. **102**, 226401 (2009)
38. Giannozzi, P., Andreussi, O., Brumme, T., Bunau, O., Nardelli, M.B., Calandra, M., Car, R., Cavazzoni, C., Ceresoli, D., Cococcioni, M.: Advanced capabilities for materials modelling with Quantum ESPRESSO. J. Phys.: Condens. Matter **29**, 465901 (2017)
39. Murnaghan, F.D.: The compressibility of media under extreme pressures. Proc. Natl. Acad. Sci. **30**, 244–247 (1944)
40. Zhou, F., Liu, Y., Wang, J., Kuang, M., Yang, T., Chen, H., Wang, X., Cheng, Z.: Intersecting topological nodal ring and nodal wall states in superhard superconductor FeB 4. Phys. Rev. Mater. **5**, 074201 (2021)

41. Yang, T., Jin, L., Liu, Y., Zhang, X., Wang, X.: Spin-polarized type-II nodal loop and nodal surface states in hexagonal compounds X TiO 2 (X= Li, Na, K, Rb). Phys. Rev. B **103**, 235140 (2021)
42. Zhou, F., Cui, C., Wang, J., Kuang, M., Yang, T., Yu, Z.-M., Wang, X., Zhang, G., Cheng, Z.: Perovskite-type YRh 3 B with multiple types of nodal point and nodal line states. Phys. Rev. B **103**, 245126 (2021)
43. Wang, J., Yuan, H., Liu, Y., Wang, X., Zhang, G.: Multiple dimensions of spin-gapless semiconducting states in tetragonal Sr 2 CuF 6. Phys. Rev. B **106**, L060407 (2022)
44. Wang, S., Ren, C., Li, Y., Tian, H., Lu, W., Sun, M.: Spin and valley filter across line defect in silicene. Appl. Phys. Express **11**, 053004 (2018)
45. Wang, S., Zhang, P., Ren, C., Tian, H., Pang, J., Song, C., Sun, M.: Valley hall effect and magnetic moment in magnetized silicene. J. Superconduct. Nov. Magnet. **32**, 2947–2957 (2019)
46. Galanakis, I., Mavropoulos, P.: Spin-polarization and electronic properties of half-metallic Heusler alloys calculated from first principles. J. Phys.: Condens. Matter **19**, 315213 (2007)
47. Faid, F., Elchikh, M., Bahlouli, S., Kaddar, K.: Strong correlation effect in ferrimagnetic half-metallic v2CoAl and V2CoGa Heusler compounds. J. Superconduct. Nov. Magnet. **31**, 2491–500 (2018)
48. Galanakis, I., Mavropoulos, P., Dederichs, P.H.: Electronic structure and Slater-Pauling behaviour in half-metallic Heusler alloys calculated from first principles. J. Phys. D Appl. Phys. **39**, 765 (2006)
49. Slater, J.C.: Wave functions in a periodic potential Physical Review **51**, 846 (1937)
50. Pauling, L.: The nature of the interatomic forces in metals Physical Review **54**, 899 (1938)
51. Rai, D., Shankar, A., Ghimire, M., Thapa, R.: Electronic and magnetic properties of a full-Heusler alloy Co2CrGe: a first-principles study. J. Theor. Appl. Phys. **7**, 1–6 (2013)
52. Pugh, S.: XCII Relations between the elastic moduli and the plastic properties of polycrystalline pure metals. The London, Edinburgh, and Dublin Philos. Mag. J. Sci. **45** 823–43 (1954)
53. Frantsevich, I.N.: Elastic constants and elastic moduli of metals and insulators Reference book (1982)
54. Hill, R.: The elastic behaviour of a crystalline aggregate. Proc. Phys. Soc. Sect. A **65**, 349 (1952)
55. Lewandowski, J., Wang, W., Greer, A.: Intrinsic plasticity or brittleness of metallic glasses. Philos. Mag. Lett. **85**, 77–87 (2005)
56. Yan, J., Shou, H., Peng, M., Duan, Y., Cao, Y.: The anisotropic properties and Debye temperatures of Ti-Zn compounds: a first-principles calculation Materials Research Express **6**, 116528 (2019)
57. Alarco, J.A., Mackinnon, I.D.: Phonon dispersions as indicators of dynamic symmetry reduction in superconductors *Phonons in Low Dimensional Structures*, pp. 75–101. InTech Open, London UK (2018)
58. Feng, D., Jin, G.: Introduction To Condensed Matter Physics, Volume 1: World Scientific Publishing Company) (2005)
59. Gueddouh, A.: Magnetic moment collapse induced by high-pressure in semi-borides TM2B (TM= Fe, Co). A first-principles study Chinese Journal of Physics **56**, 944–957 (2018)
60. Rougab, M., Gueddouh, A.: Light doping effects of rare-earth elements: Sc, Y, La and Lu in rockSalt AlN—first-principles study. Appl. Phys. A **127**, 1–11 (2021)
61. Baroni, S., De Gironcoli, S., Dal Corso, A., Giannozzi, P.: Phonons and related crystal properties from density-functional perturbation theory Reviews of modern physics **73**, 515 (2001)
62. Yang, T., Xie, C., Chen, H., Wang, X., Zhang, G.: Phononic nodal points with quadratic dispersion and multifold degeneracy in the cubic compound Ta 3 Sn . Phys. Rev. B **105**, 094310 (2022)
63. Xie, C., Yuan, H., Liu, Y., Wang, X.: Two-nodal surface phonons in solid-state materials. Phys. Rev. B **105**, 054307 (2022)
64. Ding, G., Zhou, F., Zhang, Z., Yu, Z.-M., Wang, X.: Charge-two Weyl phonons with type-III dispersion. Phys. Rev. B **105**, 134303 (2022)
65. Zhong, M., Han, Y., Wang, J., Liu, Y., Wang, X., Zhang, G.: Material realization of double-Weyl phonons and phononic double-helicoid surface arcs with P 2 1 3 space group. Phys. Rev. Mater. **6**, 084201 (2022)
66. Zhou, F., Chen, H., Yu, Z.-M., Zhang, Z., Wang, X.: Realistic cesium fluogermanate: an ideal platform to realize the topologically nodal-box and nodal-chain phonons. Phys. Rev. B **104**, 214310 (2021)
67. Wang, J., Yuan, H., Kuang, M., Yang, T., Yu, Z.-M., Zhang, Z., Wang, X.: Coexistence of zero-, one-, and two-dimensional degeneracy in tetragonal SnO 2 phonons . Phys. Rev. B **104**, L041107 (2021)
68. Zhou, F., Zhang, Z., Chen, H., Kuang, M., Yang, T., Wang, X.: Hybrid-type nodal ring phonons and coexistence of higher-order quadratic nodal line phonons in an AgZr alloy. Phys. Rev. B **104**, 174108 (2021)
69. Zhong, M., Liu, Y., Zhou, F., Kuang, M., Yang, T., Wang, X., Zhang, G.: Coexistence of phononic sixfold, fourfold, and threefold excitations in the ternary antimonide Zr 3 Ni 3 Sb 4. Phys. Rev. B **104**, 085118 (2021)